Electromagnetic Scattering Problem Solving by an Integral Meshless-Based Approach

Williams L. Nicomedes[1], Renato C. Mesquita[2], Fernando J. S. Moreira[1]

Federal University of Minas Gerais, Dept. of Electronics Engineering (1) and Dept. of Electrical Engineering (2)
Belo Horizonte, Brazil
wlnicomedes@yahoo.com.br, renato@ufmg.br, fernandomoreira@ufmg.br

***Abstract* – The present work evaluates the application of a meshless-based method to a set of integral equations arising in electromagnetic field scattering problems. These integral equations are discretized via the Moving Least Squares (MLS) approximation. The problem concerning the scattering of a TM plane wave by an infinite conductor cylinder is solved. Results show that the obtained meshless method presents good precision and fast convergence to the solution.**

I. INTRODUCTION

In electrodynamics, particularly in its branch related to the study of high frequency fields, it is a common practice to employ the Method of Moments (MoM) as an aid to obtain precise numerical solutions to integral equations related to scattering phenomena [1]. Meshless methods have successfully been applied as a feasible alternative to the Finite Element Method (FEM) in static [2], [3] and low frequency problems [4]. Recently, they have also been applied to solve electromagnetic scattering problems [5]. In all the above applications, the weak form of the problem has been discretized using the Element-Free Galerkin method. In this paper we provide another approach: we directly discretize the integral equations arising in electrodynamics.

II. THE MESHLESS APPROACH

A. Presentation

The meshless approach begins by spreading nodes over the domain of the problem to be solved. Nodes are simple points and to each one a shape function is associated. Each shape function has the property of being zero over the whole domain, except in the vicinity of the corresponding node. The vicinal region in which the shape function is different from zero is the node's *influence domain* [2]. The main difference between meshless methods and mesh-based methods (like the FEM) is that the *element* concept is not present. The influence domains are arbitrary (the only restriction is that the set of influence domains must cover the entire domain) and can overlap. So, the nodes can be distributed arbitrarily without generating an element mesh.

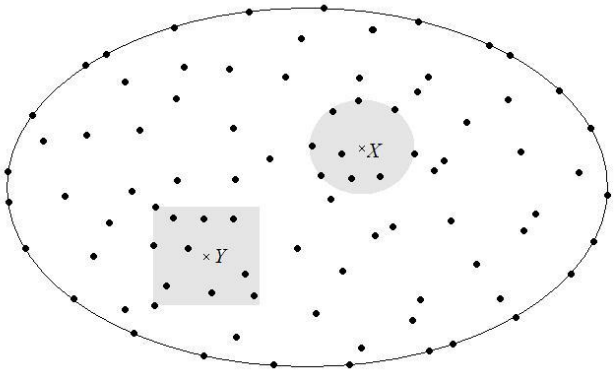

Fig.1 Nodes spread in a domain. Those ones that influence points X and Y are shown as belonging to regions that surround these points (shaded regions).

For a given point (e.g. point $\vec{x} = X$ in Fig. 1), an unknown solution u is expressed as a sum of the contributions of those nodes that influence X, i.e. nodes that extend their influence domains onto X (they are depicted inside the circular shaded region):

$$u(\vec{x}) \sim u^h(\vec{x}) = \sum_{i=1}^{N} \phi_i(\vec{x})\hat{u}_i = \boldsymbol{\Phi}(\vec{x})\boldsymbol{u} \qquad (1)$$

where u^h is the approximated solution, N is the number of nodes whose influence domains include the point $\vec{x}$, each ϕ_i is the i-th node shape function evaluated at $\vec{x}$, and $\hat{u}_i$ is the associated nodal parameter.

B. Shape Function Construction

As there is no mesh to support the shape function construction, they are built using the Moving Least Squares (MLS) approximation [2]. In the MLS, u^h is expressed as:

$$u^h(\vec{x}) = \sum_{j=1}^{m} p_j(\vec{x})a_j(\vec{x}) = \boldsymbol{p}^T(\vec{x})\boldsymbol{a}(\vec{x}) \qquad (2)$$

where $\boldsymbol{p}$ is a monomial basis with m terms (e.g. $\boldsymbol{p}(\vec{x}) = [1, x, y]$) and $\boldsymbol{a}$ is a vector of coefficients which are functions of $\vec{x}$. We then build a slightly different approximation, by requiring the monomial basis to be calculated at each node:

$$u^h(x,\vec{x}_i) = \sum_{j=1}^{m} p_j(\vec{x}_i)a_j(\vec{x}) = \boldsymbol{p}^T(\vec{x}_i)\boldsymbol{a}(\vec{x}) \quad (3)$$

The next step is to define a weighted functional M:

$$M = \sum_{i=1}^{N} w\left(\frac{\|\vec{x}-\vec{x}_i\|}{d_i}\right)[u^h(\vec{x},\vec{x}_i) - \hat{u}_i]^2 \quad (4)$$

or

$$M = \sum_{i=1}^{N} w\left(\frac{\|\vec{x}-\vec{x}_i\|}{d_i}\right)\left[\sum_{j=1}^{m} p_j(\vec{x}_i)a_j(\vec{x}) - \hat{u}_i\right]^2 \quad (5)$$

where d_i is the size of the influence domain associated to node i and w is a function with compact support centered in node i. We have chosen it to be a cubic spline [2]:

$$w = \begin{cases} 2/3 - 4r^2 + 4r^3 & ,0 \le r \le 0.5 \\ 4/3 - 4r + 4r^2 - 4/3\, r^3 & ,0.5 < r \le 1 \\ 0 & ,r > 1 \end{cases} \quad (6)$$

where $r = \|\vec{x}-\vec{x}_i\|/d_i$. Looking for the coefficients a_j that minimize the functional, we have imposed

$$\frac{\partial M}{\partial \boldsymbol{a}} = 0 \quad (7)$$

After some matrix manipulation, we obtain

$$\boldsymbol{a}(\vec{x}) = [\boldsymbol{A}(\vec{x})]^{-1}[\boldsymbol{B}(\vec{x})]\boldsymbol{u} \quad (8)$$

where

$$\boldsymbol{u}^T = [\hat{u}_1, \hat{u}_2, \dots, \hat{u}_N] \quad (9)$$

$$\boldsymbol{A}(\vec{x}) = \boldsymbol{P}^T\boldsymbol{W}(\vec{x})\boldsymbol{P} \quad (10)$$

$$\boldsymbol{B}(\vec{x}) = \boldsymbol{P}^T\boldsymbol{W}(\vec{x}) \quad (11)$$

which are given in terms of

$$\boldsymbol{P} = \begin{bmatrix} p_1(\vec{x}_1) & \cdots & p_m(\vec{x}_1) \\ \vdots & \ddots & \vdots \\ p_1(\vec{x}_N) & \cdots & p_m(\vec{x}_N) \end{bmatrix} \quad (12)$$

$$\boldsymbol{W}(\vec{x}) = \begin{bmatrix} w\left(\frac{\|\vec{x}-\vec{x}_1\|}{d_1}\right) & \cdots & 0 \\ \vdots & \ddots & \vdots \\ 0 & \cdots & w\left(\frac{\|\vec{x}-\vec{x}_N\|}{d_N}\right) \end{bmatrix} \quad (13)$$

By equating the expressions (1) and (2) the shape functions are readily available:

$$\boldsymbol{\Phi}(\vec{x}) = [\phi_1(\vec{x}), \dots, \phi_N(\vec{x})] = \boldsymbol{p}^T\boldsymbol{A}^{-1}(\vec{x})\boldsymbol{B}(\vec{x}) \quad (14)$$

III. SCATTERING ANALYSIS

A. Integral Equations

The problem to be analyzed is that of a normally incident monochromatic TM^z plane wave scattered by an infinite perfectly electric conductor (PEC) cylinder. The scattered field can be evaluated after the induced surface electric current density J_s is determined. For a cylinder infinite in the z-direction, along which the current flows ($J_s \to J_z$), no quantity is dependent upon z. Hence, the problem is two-dimensional and the calculations are made only regarding the cylinder cross-section. The incident TM plane wave, coming from the left and having only the z-component is:

$$E_z^i(\vec{x}) = E_z^i(x,y) = E_0 e^{-jkx} \quad (15)$$

where E_0 is an amplitude constant and $k = 2\pi/\lambda$ is the wavenumber (λ being the wavelength).

Two integral equations are cast for the numerical solution of the scattering problem. By reasoning about the electric field, from the boundary condition for the total field (incident and scattered)

$$E_z^i(\vec{x}) + E_z^s(\vec{x}) = 0 \; at \; the \; cylinder \; surface \quad (16)$$

and from the expression for the scattered field [1]

$$E_z^s(\vec{x}) = \left(\frac{\nabla\nabla\cdot + k^2}{j\omega\varepsilon}\right)\oint J_z(\vec{x}')H_0^{(2)}(kR)dl' \quad (17)$$

one obtains the Electric Field Integral Equation (EFIE):

$$E_z^i(\vec{x}) = \frac{\omega\mu}{4}\oint J_z(\vec{x}')H_0^{(2)}(kR)dl' \quad (18)$$

where $\vec{x}$ and $\vec{x}'$ locate the observation and source points at the cylinder cross-section perimeter, respectively, $R = \|\vec{x}-\vec{x}'\|$, $\omega = 2\pi f$, where f is the wave frequency, ε is the permittivity of the medium, and $H_0^{(2)}$ is the zero-order Hankel function of the second type. The integral (18) is to be evaluated over the entire perimeter of the cross-section.

By reasoning about the magnetic field, from the boundary condition (also at the cylinder surface)

$$\hat{\boldsymbol{n}} \times \left[\vec{H}^i(\vec{x}) + \vec{H}^s(\vec{x})\right] = \vec{J}_s(\vec{x}) = \hat{\boldsymbol{z}}J_z(\vec{x}) \quad (19)$$

and from the expression for the scattered field [1]

$$\vec{H}^s(\vec{x}) = \nabla \times \hat{\boldsymbol{z}}\oint J_z(\vec{x}')H_0^{(2)}(kR)dl' \quad (20)$$

the Magnetic Field Integral Equation (MFIE) is obtained:

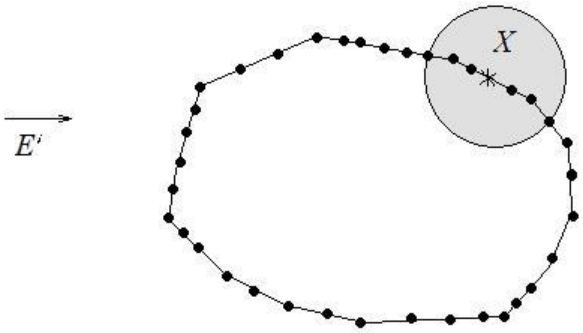

Fig. 2 Nodes at the cylinder cross-section boundary.

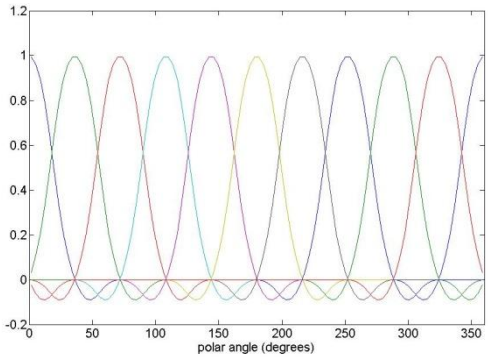

Fig. 3 A set of 10 shape functions for a circular cross-section.

$$\hat{\boldsymbol{n}} \times \vec{H}^i(\vec{x}) = \hat{\boldsymbol{z}} J_z(\vec{x}) - \hat{\boldsymbol{n}} \times \nabla \times \hat{\boldsymbol{z}} \oint J_z(\vec{x}') H_0^{(2)}(kR) dl' \tag{21}$$

In principle, both EFIE and MFIE can be used to solve for J_z. However, spurious resonant solutions may come into the scene and compromise the precision of the numerical evaluation, especially for an electrically large cylinder cross-section [1]. The resonance problem can be avoided by a linear combination of (18) and (21):

$$CFIE = \alpha\, EFIE + (1-\alpha)\, \eta\, MFIE \tag{22}$$

where α is a parameter ranging from zero to one and η is the intrinsic impedance of the exterior medium. Equation (22) is the Combined Field Integral Equation (CFIE) and α is generally set equal to 0.5 [1].

B. CFIE Meshless Numerical Solution

The problem at hand consists of numerically evaluating the surface integral equation (22) in order to obtain the surface electric current J_z. Nodes are then spread along the perimeter of the cylinder cross section (Fig. 2). Figure 3 illustrates the shape functions for 10 uniformly spaced nodes distributed along the contour. Expressing the surface current as a sum of shape functions built through the MLS approximation there follows:

$$J_z(\vec{x}) = \sum_{i=1}^{N} \phi_i(\vec{x}) \hat{u}_i \tag{23}$$

Taking the CFIE (22) for each observation point $\vec{x}_i$ (locus of the node i, determined by its polar angle φ_i) and applying (23) to represent J_z in (22), we get the following linear system in $\boldsymbol{u}$:

$$\sum_{j=1}^{N} K_{ij}^c \hat{u}_j = f_i^c \tag{24}$$

where

$$K_{ij}^c = \alpha K_{ij}^e + (1-\alpha)\eta K_{ij}^m \tag{25}$$

$$f_i^c = \alpha f_i^e + (1-\alpha)\eta f_i^m \tag{26}$$

$$K_{ij}^e = \frac{\omega\mu}{4} \oint \phi_j(\vec{x}') H_0^{(2)}(kR) dl' \tag{27}$$

$$K_{ij}^m = \frac{1}{2}\phi_j(\vec{x}_i) + \frac{jk}{4} \oint \phi_j(\vec{x}') H_1^{(2)}(kR) \left[\hat{\boldsymbol{n}} \cdot \hat{R}\right] dl' \tag{28}$$

$$f_i^e = E_z^i(\vec{x}_i) \tag{29}$$

$$f_i^m = \left\{\hat{n} \times \vec{H}_i(\vec{x}_i)\right\}.\hat{z} \tag{30}$$

and $H_1^{(2)}$ is the first order Hankel function of the second type. In (28) and (30), the coefficients have been obtained from (21) after some vector manipulation. Once the $\hat{u}_i$ parameters are found, the surface current density at a given $\vec{x}$ can be determined by first finding the nodes that influence $\vec{x}$ and then applying (23). K^c is symmetrical, but it is not sparse. This shortcoming is due to the fact that the Hankel functions centered at a node extend over the whole domain, thus making any coefficient K_{ij}^c different from zero.

IV. NUMERICAL RESULTS

In order to evaluate the convergence of the method, we have chosen the scattering of a plane wave by a circular perfect electric conductor (PEC) cylinder. This problem possesses analytical solution, thus providing means to study the precision of the numerical results. The scattering equations can be specialized for a circular cylinder through use of polar coordinates (ρ, φ) to locate a point at the cylinder surface. As the radius of the cross section is constant $(\rho = a)$, the equations become functions of φ alone. Figure 4 illustrates the geometry of the problem.

At the cylinder surface $\rho = a$, the incident field is expressed as:

$$E_z^i(\vec{x}) = E_z^i(\vec{\rho}) = E_z^i(\rho, \varphi) = E_z^i(\varphi) = E_0 e^{-jka\cos\varphi} \tag{31}$$

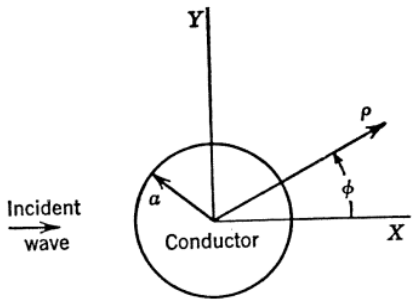

Fig. 4 Problem geometry; circular cylinder cross-section.

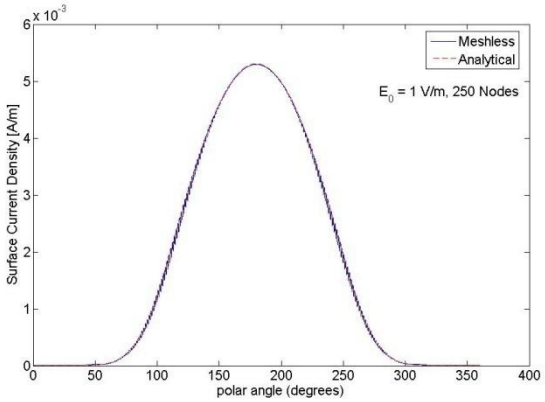

Fig. 5 Surface current modulus for a PEC circular cylinder, radius $a = 10\lambda$. 250 nodes have been spread along the contour during the analysis.

In performing the plane-wave scattering analysis for a PEC cylinder with radius $a = 10\lambda$ and for an incoming plane wave having unit amplitude, the number of nodes uniformly distributed over the circular perimeter was gradually increased from 10 to 600. It was found that when the number of nodes is greater than 100, the solution begins to converge, when compared to the analytical solution [6]:

$$J_z(\vec{\rho}) = \frac{2E_0}{\pi a \omega \mu} \sum_{n=-\infty}^{+\infty} j^{-n} \frac{e^{jn\varphi}}{H_n^{(2)}(ka)} \qquad (32)$$

where φ is the observation angle along the circular contour and $H_n^{(2)}$ is the n-th order Hankel function of the second type. Figure 5 shows the comparison between the current amplitude obtained from the meshless method (for 250 uniformly distributed nodes) and its analytical expression (32) as a function of φ. From Fig. 5 one observes that both curves are almost indistinguishable.

To study the numerical convergence of the proposed procedure, the following RMS norm was used as a measure of the error between the numerical and analytical solutions:

$$norm = \sqrt{\frac{1}{2\pi a} \oint \left[J_{z_{Analytical}} - J_{z_{Numerical}} \right]^2 dl'} \qquad (33)$$

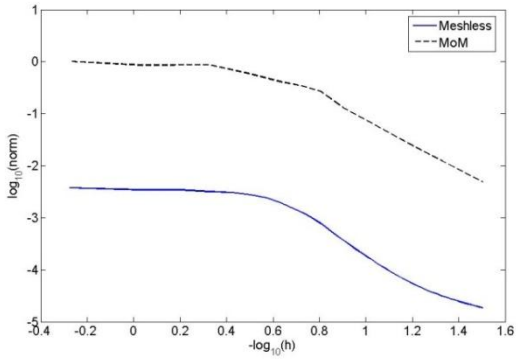

Fig.6 Convergence of the error norm for the messless approach and for a MoM analysis employing pulse expansion functions and point-matching.

Figure 6 shows a log-log plot of the error norm as a function of the discretization length h, where h is the distance between two consecutive nodes along the circular contour. A linear regression applied to the rectilinear portion of the graph (abscissa between 0.8 and 1.1) shows that the convergence rates are approximately 3.07 for the meshless method and 2.66 for MoM, when the CFIE is employed. Besides that, the meshless approach provides a smaller RMS error norm. Away from the cylinder internal resonances, [7] provides the convergence rates for the RMS current error calculated through MoM. For a flat facet mesh with pulse expansion and delta testing functions (point matching), these are approximately 2 for the EFIE and 1 for MFIE alone [7].

V. CONCLUSIONS

In this work we have analyzed the plane-wave scattering by a PEC cylinder using surface integral equations numerically evaluated by a meshless-based method. The results obtained show that the numerical solution based on a meshless approach converges to the analytical solution in a satisfactory way. As we have employed a surface integral formulation, the resulting matrix K^c is not sparse, although symmetrical.

REFERENCES

[1] A. Peterson, S. Ray, and R. Mittra, *Computational Methods for Electromagnetics*, IEEE Press, 1998.

[2] G. Liu, *Mesh Free Methods: Moving Beyond the Finite Element Method*, CRC Press, 2002.

[3] G. Parreira, E. Silva, A. Fonseca, and R. Mesquita, "The Element-free Galerkin Method in 3-Dimensional Electromagnetic Problems", *IEEE Transactions on Magnetics*, vol. 42, no. 4, pp. 711-714, 2006.

[4] O. Bottauscio, M. Chiampi, and A. Manzin, "Element-free Galerkin method in eddy-current problems with ferromagnetic media", *IEEE Transactions on Magnetics*, vol. 42, no 5, pp. 1577-1584, 2006.

[5] A. Manzin, and O. Bottauscio, "Element-free galerkin method for the analysis of electromagnetic-wave scattering", *IEEE Transactions on Magnetics*, vol. 44, no 6, pp. 1366-1369, 2008.

[6] C. Balanis, *Advanced Engineering Electromagnetics*, John Wiley & Sons, 1989.

[7] C. Davis and K. Warnick, **"**Convergence rates of 2D moment method solutions for the MFIE and EFIE", *IEEE Antennas and Propagation Society International Symposium*, Columbus, OH, pp. 1080-1083, June 2003.